LIMNOLOGY
and
OCEANOGRAPHY: METHODS

Limnol. Oceanogr.: Methods 12, 2014, 484–497

Characterization and field test of an in situ multi-platform optical sensor

Chee-Loon Ng[1], Wei-Kiat Teo[1], Hui-Ting Cai[1], and Harold F. Hemond[2]*

[1]Center for Environmental Sensing and Modeling, Singapore-MIT Alliance for Research and Technology Centre, CREATE Tower Level 9, Singapore 138602

[2]Department of Civil and Environmental Engineering, Building 48, Massachusetts Institute of Technology, Cambridge, MA, USA 02139

Abstract

The characterization and field testing of a compact in situ optical instrument using fluorescence, absorbance, and scattering to identify and quantify contaminants and natural substances in water bodies are described. The instrument, based on a technology named LEDIF (LED-Induced Fluorescence) developed by Ng et al. (2012*a*) was configured for in situ long-term continuous monitoring at a fixed location. The optical performance and sensing capabilities of the instrument were assessed by calibrating against laboratory-prepared and commercial standards, and compared with several commercial sensors and published values. The effects on sensor response of temperature, pressure, and particle interference due to turbidity and total suspended solids were assessed and reported. Instrumental baseline shift over time, instrument detection limits, and the capability of LEDIF to determine characteristics such as quantum yield and intramolecular deactivation of fluorescence response, were also assessed. Experimental results match well with results from commercial instruments and published data. To demonstrate field deployment, the LEDIF instrument was installed at Chinese Garden of Singapore for long-term continuous monitoring of chlorophyll *a* (Chl *a*) and turbidity at a management-selected location. The analytes were chosen based on management's needs in recording temporal trends of algal biomass and water cloudiness to develop effective controls of inflow and outflow water quality. A monitoring record showing the temporal response of algal biomass to ambient conditions and turbidity variations is presented and discussed.

Understanding of water chemistry via laboratory analysis of collected samples is time consuming and costly, and samples may degrade due to time delay in transport. Sample collection followed by laboratory analysis also puts practical limits on the number of measurements that can be made, potentially resulting in failure to capture spatiotemporal variability or temporal trends that may assist in understanding biogeochemical processes in water bodies. Monitoring requirements may generally be classified as short-term, long-term, or continuous. Short-term monitoring that has a specific purpose may be intensive but finite in duration, whereas long-term monitoring focuses on establishing the status and trends of the water bodies. Continuous monitoring may be needed if it is desired to trigger immediate counteractive responses in the management and operation of important water resources.

*Corresponding author: E-mail: kelvinng@smart.mit.edu

Acknowledgments

Full text appears at the end of the article.

DOI 10.4319/lom.2014.12.484

Literature on in situ sensing of water chemistry has been reviewed by Ng et al. (2012*b*) and literature cited therein. As such, the review in this article will be brief and will focus on long-term continuous monitoring. Long-term continuous monitoring can take the form of a single sensor or sentinel sensor network placed at a location of interest to understand temporal patterns of water chemistry, and in some cases, trigger counteractive responses when certain parameters fall outside acceptable limits for safeguarding of water resources. Storey et al. (2011) reviewed online monitoring technology for the detection of contaminants in water, based on their visits to water utilities, research organizations, and technology throughout Europe, United States, and Singapore. They compared and summarized the advantages and limitations of the following sensing technologies: J-Mar Biosentry (U.S. EPA 2010), UV-VIS s::an spectro::lyser (van den Broeke 2005; U.S. EPA 2010), Hach Guardian Blue (Hohman 2007), YSI Sonde (Atkinson and Mabe 2006), Censar (U.S. EPA 2009), s::can Water Quality Monitoring Station (Chow et al. 2008), MicroLAN TOXControl (Zurita et al. 2007; Mons 2008), BBE Algae Toximeter (de Hoogh et al. 2006; Mons 2008), BBE Daphnia Toximeter (de Hoogh et al. 2006; Jeon et al.

2008; Mons 2008), BBE ToxProtect (van der Gaag and Volz 2008; Mons 2008), ZWEEC Analytics FAMS (van der Gaag and Volz 2008; Mons 2008), surface-enhanced Raman spectroscopy (Sengupta et al. 2006; van der Gaag and Volz 2008), laser tweezer Raman spectroscopy (Xie et al. 2005; van der Gaag and Volz 2008), surface acoustic wave (SAW) devices (van der Gaag and Volz 2008). They conclude that there is no universal monitor for water quality monitoring and contaminant detection, an unsurprising result given the multiplicity of substances that may be of concern. Sensors for traditional water quality parameters (e.g., pH, temperature, among others) continue to provide reliable information but monitoring needs for other parameters evolve to meet operational demands. Storey et al. (2011) call for evolution resulting in sensing technology that is less expensive, more reliable, easier to implement, and provides real-time wireless access. Sensors suitable for monitoring a wide range of water bodies (rivers, ponds, among others) are especially important in a nation like Singapore that has limited resources of freshwater.

A multi-platform optical sensing device for in situ sensing of water chemistry has been described by Ng et al. (2012*a*). Ng et al. (2012*b*) demonstrate the packaging and the use of the device aboard an autonomous underwater vehicle to provide three-dimensional (3-D) chemical mapping. In this work, characterization and field testing of the sensing device as adapted for long-term continuous monitoring are described.

Materials and procedure

Sensor module

The layout of PORTA LEDIF and its field deployment are shown in Fig. 1. The optical functions of PORTA LEDIF rely on a compact [~37(W) × 61(L) mm] custom-designed flowcell having six junctions fitted with light emitting diodes (LEDs) of different wavelengths, focused on the analytical volume and oriented 90° from the main axis of light collection by a series of adjustable optics for fluorescence measurement. A collector lens, with focal length equal to the distance from the lens to the optical intersection with the perpendicular excitation optical paths, is fitted in front of the detecting optic junction to enhance collection of light emitted by fluorescence. The optic junctions use UV-transmissive fused silica windows with O-ring seals. Absorbance is measured using a broadband (185 nm to 1100 nm) light source coupled via an optical fiber; a collimation lens illuminates the flowcell at 180° to the light collection system. Turbidity is also measured within the flowcell using nephelometry, at each LED wavelength. Fluid flow into the flowcell occurs via a pathway that contains two 90° bends to minimize the entrance of stray light.

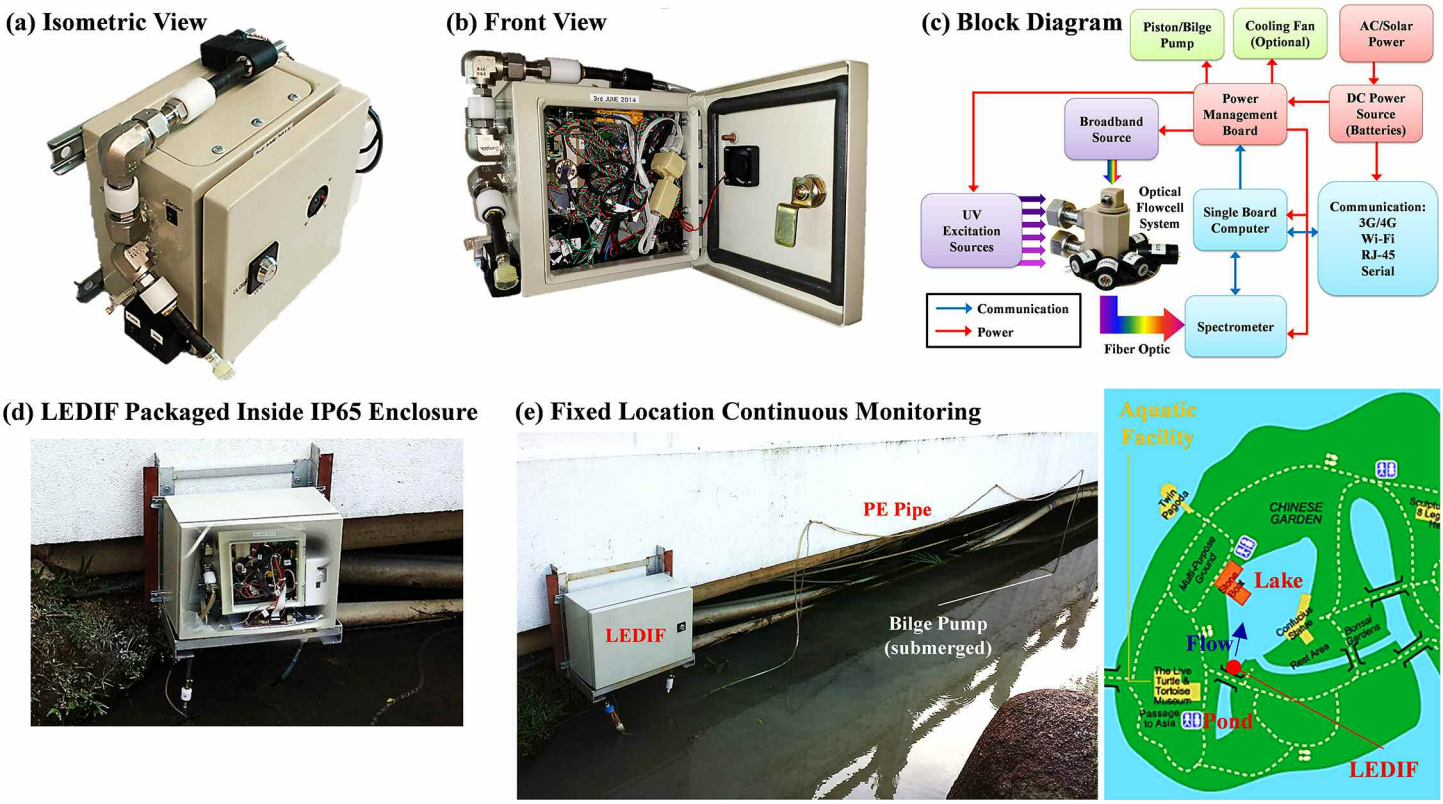

Fig. 1. The layout of the LEDIF and its field deployment: (a and b) isometric and front views of LEDIF packaged inside a 20 × 15 × 20 cm enclosure for portable mode sensing, (c) LEDIF block diagram, (d) LEDIF and supplementary components packaged inside an IP65 40 × 30 × 20 cm enclosure mounted onto an external bracket on the test site for long-term continuous monitoring, and (e) photo of field deployment and map of sampling location.

For all measurements, light from the flowcell is observed with an Ocean Optics USB4000 spectrometer, and the data are recorded with a single board computer manufactured by Technologic Systems (Model TS-7260-64-128F) running custom software (iLEDLIF) under a Debian Linux operating system that controls the sensor functionalities and handles all communication with external devices via serial, RJ-45, wifi, and 3G/4G communications. Wifi and 3G/4G communications are enabled via a TP-LINK 3G/4G Portable Wireless N Router (Model: TL-MR3020) coupled with a TP-LINK 3.75G HSUPA USB adapter (Model: MA180) equipped with a 3G/4G SIM Card and data bundle subscription. PORTA LEDIF uses switching DC-DC converters to efficiently provide 5 and 12 VDC to various subsystems from an internal battery and/or from an external power supply voltage between 12 and 72 VDC. A 5 VDC fan helps regulate the temperature of PORTA LEDIF to enhance the stability of sensor response. A compact 12 VDC Gotec (Model: EMX-08) piston pump is used to feed sample into the LEDIF flowcell manifold. A low-cost SEAFLO (Model: SFBP1-G350-01) submersible bilge pump connected to polyethylene (PE) tubing is used to transport sample from the water body into the PORTA LEDIF flowcell manifold. A detailed description of LEDIF technology is available in Ng et al. (2012*a*) and Ng et al. (2012*b*).

The PORTA LEDIF allows sensing to be made in either nonflowing or flowing modes. For the nonflowing mode, a ball check valve is installed at the inlet of the inflow line to stop backflow after the bilge pump has been turned off. For flowing mode, measurement is made with the bilge pump running. The latter mode results in improved performance for certain measurement (e.g., algae biomass) by avoiding settling of algal cells.

Fluorescence characterization

The performance of PORTA LEDIF (hereafter LEDIF) was compared with a Shimadzu RF-5301 (S_RF-5301), a Perkin Elmer LS-55 (PE_LS-55), and published spectra from PhotoChemCAD (Du et al. 1998) for fluorescence measurements. The S_RF-5301 and PE_LS-55 are a commercially available spectrofluorophotometer and luminescence spectrometer, respectively, that use xenon lamps as the sources of excitation, and record emission spectra from 220 to 900 nm (S_RF-5301) or 200 to 900 nm (PE_LS-55), respectively. Wavelengths are selected with an excitation monochromator and an emission monochromator. For the S_RF-5301 and the PE_LS-55, the manufacturer's stated wavelength accuracy is ±1.5 nm with a maximum scanning speed of 5500 nm/min, and ±1 nm with a scanning speed of 10 to 1500 nm/min with 1 nm increments, respectively. For the S_RF-5301, the signal-to-noise ratio is stated as 150:1 and 600:1 observing the water Raman line of distilled water using 350 nm, 5 nm, and 10 nm bandwidth settings, respectively, and having a 0 to 98% response of two seconds (http://www.ssi.shimadzu.com/products/product.cfm?product = rf5301). For the PE_LS-55, the signal-to-noise ratio is stated as 2500:1 RMS at the baseline and 750:1 RMS for observing the water Raman line using 350 nm as excitation (http://www.perkinelmer.com/Catalog/Product/ID/L2250107).

Chl *a* (Tokyo Chemical Industry) was chosen as an analyte for characterization. The fluorescence emission of each instrument was normalized by the mean value of $\gamma = I_{peak(LEDIF)}/I_{peak}$, to allow comparison of spectrum profiles and fluorescence responses at different concentrations. The correlation obtained from the normalized peak intensity as a function of concentration was used to estimate the Chl *a* concentrations of field samples. LEDIF instrument shift after an elapsed time of 4 months was also assessed using freshly prepared laboratory standards.

Absorbance characterization

The performance of LEDIF in absorbance mode was compared with Ocean Optics CHEMUSB4-UV-VIS (OO) and Shidmazu UV-2550 (S_UV-2550) instruments. OO is a commercially available spectrophotometer that uses a deuterium-tungsten light source, has a 1 cm absorbance pathlength, and records absorbance spectra from 210 to 880 nm. The computed wavelength accuracy is ±7.5 nm using an aperture entrance defined by a 200 × 1000 μm slit. The signal-to-noise ratio is stated as 300:1 at full signal and the time to stabilize output after power-up is 30 min (http://www.oceanoptics.com/products/chem4uvvis.asp). S_UV-2550 is a commercially available spectrophotometer operating with a UV/VIS doubled-blazed grating and a double monochromator optical system that uses a deuterium-halogen light source, is capable of accommodating cells of different geometries and variable pathlengths, and records absorbance spectra from 190 to 900 nm. The manufacturer's stated wavelength accuracy is ±0.3 nm with automatic wavelength correction. The scanning speed is 160 to 900 nm/min with a wavelength repeatability of ±0.1 nm. (http://www.ssi.shimadzu.com/products/Lature/spectroscopy/uv-24502550.pdf).

Rhodamine B (Panreac) and fluorescein (Fluka) were chosen as sample analytes because both are tracer dyes with well quantified absorption properties. The absorbance spectra from LEDIF and OO were normalized by the product of molar absorptivity (ε) and absorbance pathlength (L) to allow comparison of spectrum profiles and absorbance responses at different concentrations. LEDIF has an absorbance pathlength of 4 cm whereas OO and S_UV-2550 have an absorbance pathlength of 1 cm. The measurements of OO and S_UV-2550 were corrected for absorbance pathlength and compared with measurements of LEDIF. The measured molar absorptivity obtained using the Beer-Lambert relationship with LEDIF data were compared with OO and S_UV-2550 results and with computed values.

Turbidity characterization

Nephelometric turbidity measurements can be made at each LED wavelength of LEDIF. LEDIF was calibrated with a standard made of styrene divinyl benzene copolymer beads in water (AMCO CLEAR TURBIDITY STANDARD manufactured by GFS Chemicals) at integration times of 100 ms and 500 ms. LEDIF was calibrated for three ranges of turbidity: (1) 0 to 1

NTU in 0.2 NTU increments, (2) 0 to 10 NTU in 2 NTU increments, and (3) 0 to 100 NTU in 20 NTU increments. These ranges are representative of samples ranging from finished drinking water to many unfiltered natural waters. 100 NTU does not reflect the upper bound limits of LEDIF, however, as higher turbidities can be measured by using shorter integration times or lower optical power. LEDIF instrument drift after an elapsed time of three months was assessed. The performance of LEDIF was compared with that of a Thermo Scientific Orion AQUAFast AQ3010 (O_AF) for linear calibration of turbidity using the same standards. O_AF is a commercial turbidity meter that uses the nephelometric principle with 90° detection, having a measurement range of 0 to 1000 nephelometric turbidity units (NTUs) and complies with the turbidity measurement technique of ISO 7027 (http://www.thermoscientific.com/en/product/orion-aquafast-aq3010-turbidity-meter.html).

Quantum yield measurement

Fluorescent quantum yield is an intrinsic property useful for applications and calculations such as fluorescence brightness and energy transfer measurements. The relative quantum yield of a fluorophore can be determined by comparing it with the quantum yield of a well-known reference fluorophore. The LEDIF's dual capability in measuring both absorbance and fluorescence allows this to be determined.

For quantum yield assessment, the comparative method of Williams et al. (1983), which involves the use of multiple characterized references with known fluorescence quantum yield, is used:

$$\Phi_f^s = \Phi_f^r \frac{F^s}{F^r}\frac{A^r}{A^s}\frac{n_s^2}{n_r^2} = \Phi_f^r \frac{m^s}{m^r}\frac{n_s^2}{n_r^2} \quad (1)$$

where $\Phi^s{}_f$ and $\Phi^r{}_f$ are the photoluminescence quantum yields of the sample and reference analyte, respectively; the subscript f signifies that it is dealing with fluorescence in this assessment. F^s and F^r are the integrated intensities (areas) of sample and reference analyte spectra, respectively (in units of photons). A^s and A^r are the absorption factors of the sample and reference analytes. n_s and n_r are the refractive indices of the sample and reference analyte.

Rhodamine 6G (reference analyte; Sigma-Alrich) and rhodamine B (sample analyte) were chosen to demonstrate quantum yield comparative measurements by LEDIF because both values are quantified in the literature. The same excitation wavelength of 525 nm was used for both sample and reference analytes; this is a common practice to prevent the introduction of uncertainty in the relative photon flux due to different excitation wavelengths, despite the fact that it is not required in principle. The procedure for determining comparative quantum yield using the LEDIF is outlined below: (1) Prepare 4 samples of rhodamine 6G and rhodamine B having different absorbances between 0.01 and 0.05 at the excitation wavelength of 525 nm. (2) Measure the fluorescence spectrum from 400 to 600 nm for the prepared standard using an excitation wavelength of 525 nm. (3) Compute the integrated fluorescence intensity from the fluorescence spectrum. (4) Plot the magnitude of the integrated fluorescence intensity as a function of absorbance obtained at the excitation wavelength of 525 nm. (5) Compute fluorescence quantum yield using Eq. 1.

Temperature and pressure effects

LEDIF is intended for in situ long-term continuous monitoring. Fluorescence is known, in general, to decrease with increased temperature (Lakowicz 2006), and the dependence varies among analytes. The experimental setup of fluorescence response to liquid temperature using LEDIF is shown in Fig. 2. The LEDIF fluid inlet and outlet were dipped into a liquid reservoir containing analyte of known concentration, and a 12 VDC Gotec (Model: EMX-08) piston pump was used to continuously circulate the analyte between LEDIF and the liquid reservoir. A temperature sensor continuously recorded the temperature of the analyte in the reservoir. The setup was put inside a temperature-regulated cold room for experiments below the reference temperature of 25°C. For experiment above the reference temperature, the liquid reservoir was put on a temperature-controlled hot plate for heating to the selected temperature.

Chl *a* and rhodamine B were chosen as analytes because the former is a pigment used to demonstrate field deployment in this article, and the latter is a tracer dye with well-defined spectroscopic properties commonly used to assess sensing device performance. The assessment was performed for both analytes at different concentrations with different excitation wavelengths and compared with temperature coefficients reported by Turner Designs (1990). For Chl *a*, fluorescence decreases linearly with the increase in temperature and can be defined as

$$\frac{I_s}{I_r} = \beta\left(\mathrm{Tmp_s} - \mathrm{Tmp_r}\right) + B \quad (2)$$

For rhodamine B, fluorescence decreases exponentially with increasing temperature and can be defined as

$$\frac{I_s}{I_r} = Be^{\beta\left(\mathrm{Tmp_s}-\mathrm{Tmp_r}\right)} \quad (3)$$

where I_s and I_r are the fluorescence peak intensities at sample and reference temperatures, respectively. $\mathrm{Tmp_s}$ and $\mathrm{Tmp_r}$ represent the sample and reference temperatures, respectively. β is the temperature coefficient and B is the intercept constant.

The effect of pressure on sensor response was assessed by making fluorescence measurements of Chl *a* with the flowcell manifold pressurized from 0 to 120 psi gauge pressure with a pressure rig.

Particle interference

Fluorescence measurement is, in general, less susceptible to particle interference than absorbance measurement. Particles that do not reflect or absorb light normally have only small effects on fluorescence measurement except at high NTU concentrations. The effect of turbidity on sensor response was assessed by mixing Chl *a* standard with styrene divinyl ben-

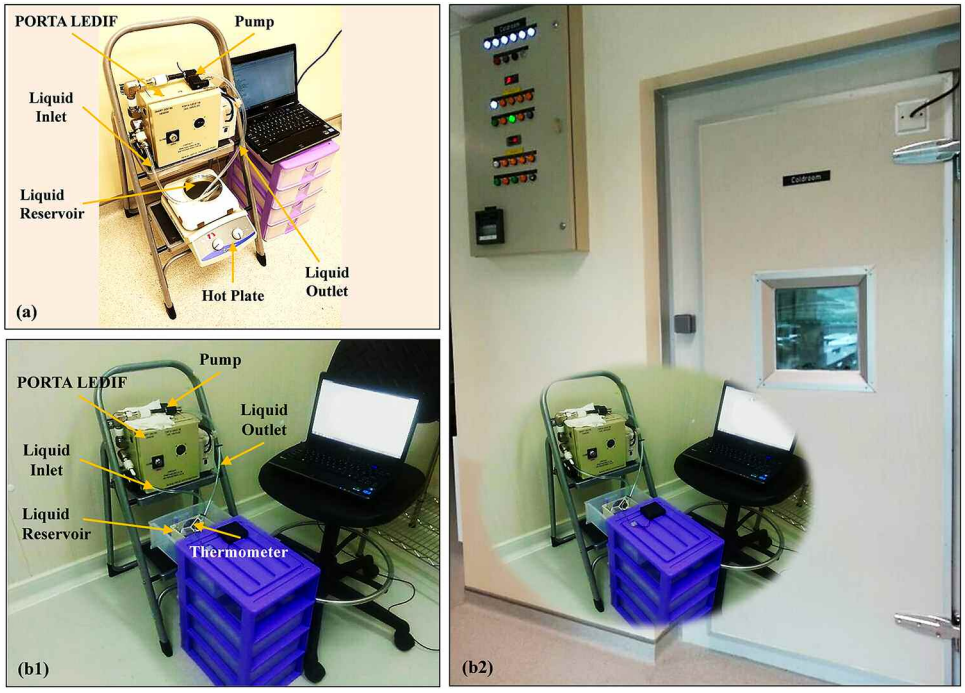

Fig. 2. Experimental setup to study temperature effect on sensor response: (a) hot plate experiment to study temperature effect above the reference temperature of 25°C and (b1 and b2) cold room experiment to study temperature effect below reference temperature of 25°C.

zene copolymer beads in water (AMCO CLEAR TURBIDITY STANDARD, GFS Chemicals) at 40 NTU, which is higher than the upper (20 NTU) value of turbidity typically observed at the current test site. The effect of total suspended solids (TSS) on sensor response was assessed by mixing Chl *a* standard with specially prepared cellulose powder in filtered ACS reagent grade water, certified traceable to the NIST national standard of mass (Ricca Chemical Comp). Again, Chl *a* was used as an analyte because it was a primary target in field deployment.

Quenching

Fluorescence is susceptible to intramolecular deactivation resulting in loss of fluorescence signal. Collision (dynamic) and complex formation (static) are two common quenching processes. In the case of collisional quenching, the quenching rate can be determined via the Stern-Volmer linear relationship defined as

$$\frac{I_f^o}{I_f} = 1 + K_{SV} \cdot [C] = 1 + k_q \tau_o \cdot [C] \quad (4)$$

where I^o_f and I_f are intensity or rate of fluorescence of the analyte sample, without and with a quencher, respectively, k_q is the quencher rate coefficient, τ_o is the lifetime of the emissive excitation state of the analyte sample, and C is the concentration of the quencher. Data on diffusion-limited quenching that permits the use of the Stokes-Einstein relation in the prediction of the quencher rate coefficient is scarce, and the true quenching rate coefficient is usually determined experimentally. Static quenching was first described by Gregorio Weber (1948); the quenching rate can be determined from

$$\frac{I_f^o}{I_f} = 1 + k_a \cdot [C] \quad (5)$$

where k_a is the association constant of the complex. In the presence of both static and dynamic quenching, the equation takes the form:

$$\frac{I_f^o}{I_f} - 1 = (k_a + K_{SV}) \cdot [C] + (k_a K_{SV}) \cdot [C]^2 \quad (6)$$

Chl *a* (sample analyte) and humic acid (quencher, Acros Organics) were chosen for these experiments because the former was the targeted analyte for field demonstration and chromophoric dissolved organic matter was present at the test site.

Long-term continuous monitoring

Long-term continuous monitoring allows temporal trends of analytes to be assessed. For field demonstration, LEDIF was deployed to Chinese Garden of Singapore (http://en.wikipedia.org/wiki/Chinese_Garden,_Singapore) for Chl *a* and turbidity measurements. Chl *a* was chosen as analyte because it is a pigment produced by algae and is commonly regarded as a proxy for algal biomass, a key parameter of aquatic systems. Turbidity was measured at the same time to determine the cloudiness of the water. The LEDIF was instrumented at a stone bridge between the pond next to an aquatic facility and the lake as shown in the map (http://www.streetdirectory.com/sg/chinese-garden-lake/56119_1.html) of Fig. 1(e). During rainy days, water flows from the pond through the stone bridge to the lake. During dry days, water flow is significantly reduced or halted. The depth of water at the sampling location was approximately one meter. Water was pumped at midwater column using a soft-

ware-controlled bilge pump and then transported via a polyethylene pipe to the LEDIF inlet. The main objectives of this field test were to verify sensor capability in capturing temporal changes of algal biomass and water cloudiness and to investigate effects of ambient conditions on the measurements. Such observations can help the management to implement effective controls and gauge the effectiveness of the solution for better maintaining the water quality on the test site.

The flowrate through the flowcell was measured to be 14.4 cm^3/s, resulting in a water velocity (V) of 62.7 cm/s in the cell, and a flow retention time of 2.4 s computed based on the flow retention time (t) equation ($t = 3V^{-1.2}$) of LEDIF published by Ng et al. (2012*b*). Although not required, the flushing time of the present work was set to be significantly higher than that of the computed value, at 75 s. LEDIF permits frequency of measurement as high as one per 10 s. A frequency of measurement of one per 7 min, later reduced to one per 23 min, was found to be sufficient to capture temporal trends at this site.

Fouling suppression

Sensors used for in situ long-term monitoring are susceptible to fouling. In the absence of any suppression device, fouling was observed to build up inside the polyethylene (PE) tubing after 2 weeks of deployment at the current field test location. This required replacement of the PE tubing and thorough cleaning of the bilge pump. Despite the fact that the fluid manifold of LEDIF is made of smooth, chemical-resistant materials, internal fouling started to interfere with sensor measurement after 8 weeks of deployment. This required the fluid manifold to be disassembled for cleaning by sonication and thorough wiping, which is labor intensive.

Copper is known to be capable of reducing fouling and hence has been used to delay sensor maintenance (Manov et al. 2003). Its fouling suppression property was applicable to the present field test location, as fouling was observed to be significantly less at various copper-containing brass fittings connected to the flowcell manifold. An anti-fouling cylindrical [~90(L) x 29(ϕ) mm] tube stuffed with copper mesh of having 5 mm hole diameter, which poses no ill effect to turbidity measurements, was attached to the outlet of the bilge pump for suppressing fouling inside the PE tubing. A second anti-fouling cylindrical tube was attached to the liquid inlet of LEDIF to enhance fouling suppression in the flowcell manifold. The copper mesh inside the anti-fouling tube was replaced on a weekly basis to ensure that sensor measurement is always maintained at good quality. The replacement can be done easily and quickly through the cap opening of the anti-fouling cylindrical tube.

Assessment

Fluorescence measurement

Fluorescence peaks were assessed by comparing fluorescence spectra of aqueous solutions of Chl *a* at different concentrations measured with LEDIF against the corresponding spectra from the S_RF-5301 and PE_LS-55, using an excitation wavelength of 405 nm (Fig. 3a). For spectrum display purposes the

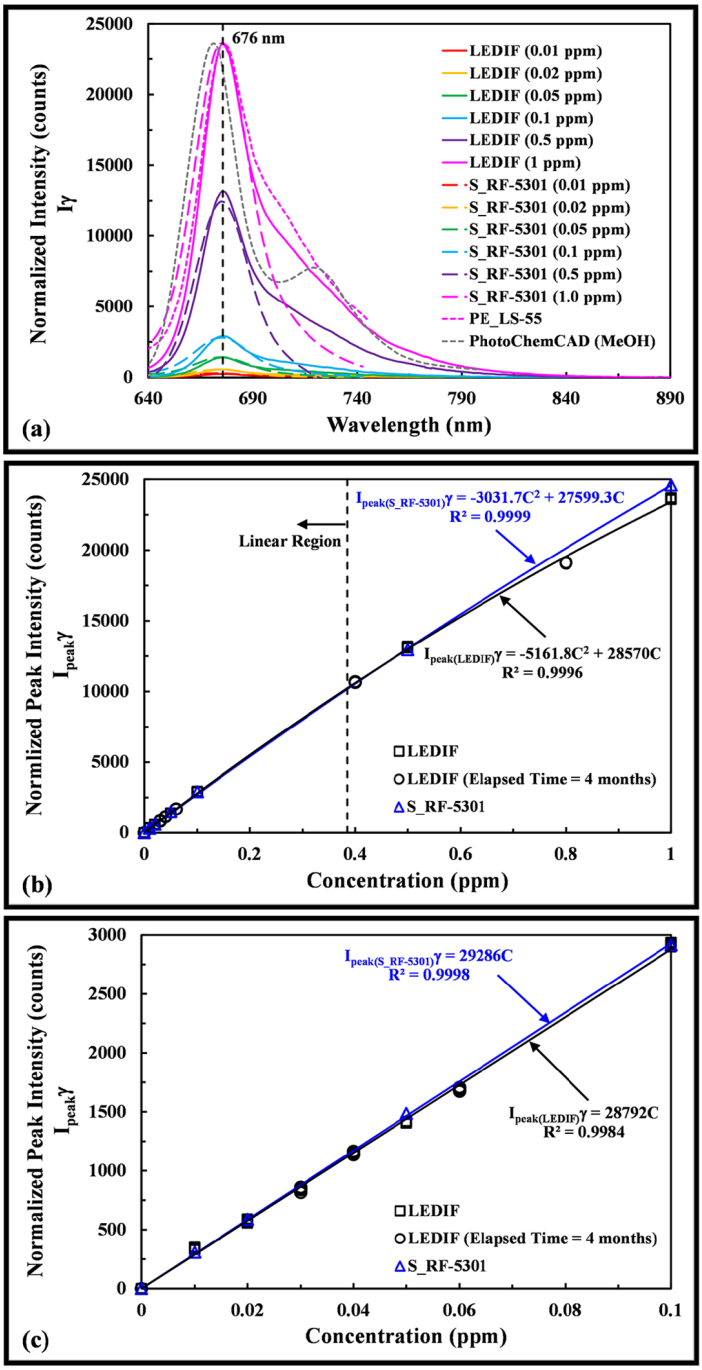

Fig. 3. (a) Fluorescence spectra of Chl *a* dissolved in water as measured by the LEDIF and by the S_RF-5301 for different concentrations. Note: Symbol legend in instrument (concentration) format. In additional to the S_RF-5301, the LEDIF spectra also match well with the spectra from the PE_LS-55 and are close to PhotoChemCAD published values (the latter in methanol MeOH) solvent, (b) measurement of normalized fluorescence peak intensity as a function of concentration for the LEDIF and the S_RF-5301. LEDIF baseline shift over an elapsed time of 4 months was immaterial, and (c) measurement of normalized fluorescence peak intensity as a function of concentration below 0.1 ppm.

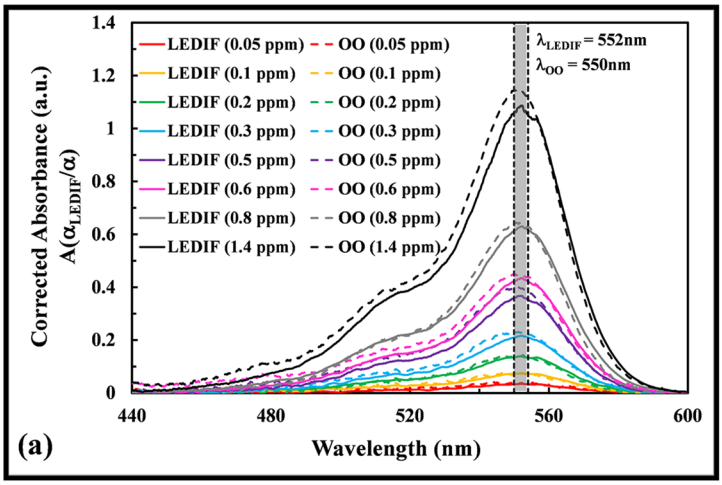

Concentration (ppm)	Molar Absorptivity (Rhodamine B)		
	LEDIF	OO	S_UV-2550
0.05	0.175	0.168	0.180
0.1	0.189	0.212	0.180
0.2	0.174	0.226	0.185
0.3	0.181	0.209	0.187
0.5	0.185	0.204	0.182
0.6	0.182	0.196	0.192
0.8	0.198	0.188	0.189
(c) 1.4	0.195	0.211	0.188

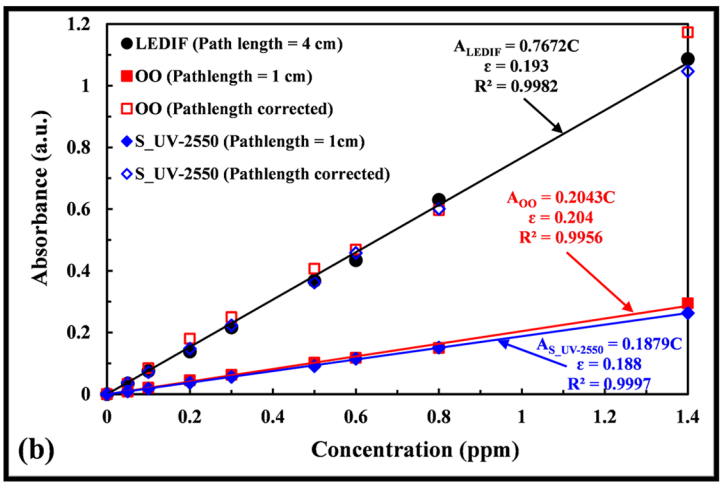

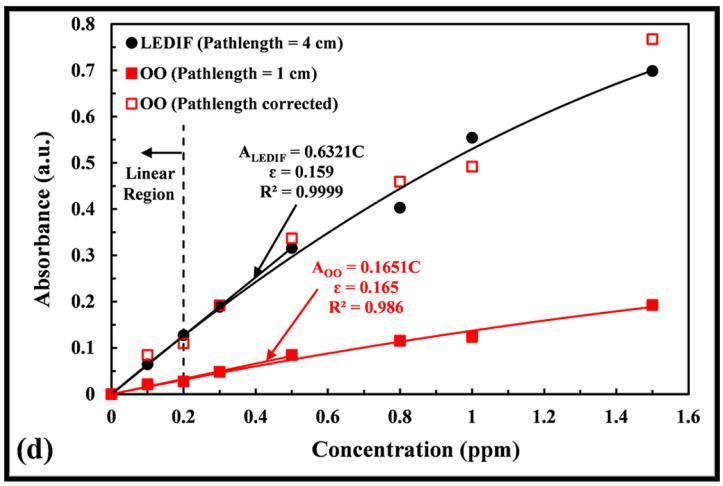

Fig. 4. (a) The absorbance spectrum of rhodamine B dissolved in water as measured by the LEDIF and the OO for different concentrations. LEDIF and OO absorbance peaks match well with the range of manufacturer's published peaks of 500 to 554 nm. Note: Symbol legend in instrument (concentration) format, (b) comparison of Beer-Lambert plots-between the LEDIF, OO, and S_UV-2550 of rhodamine B dissolved in water. OO and S_UV-2550 measurements match well with those of LEDIF after instrument pathlength (4 cm) correction. Molar absorptivity measured by LEDIF matches well with OO and S_UV-2550, (c) table showing measured and computed molar absorptivity at each concentration of the three instruments, and (d) comparison of Beer-Lambert plots between the LEDIF and the OO of fluorescein dissolved in water.

fluorescence spectrum intensities of the instruments are normalized by the mean values of γ = 1 and γ = 72.7, LEDIF and S_RF-5301, respectively. The emission peaks of Chl *a* observed by the three sensors are in excellent agreement, having differences in peak wavelength of 1.2 nm and 0.3 nm, S_RF-5301 and PE_LS-55, respectively; the fluorescence peak of Chl *a* reported by LEDIF was 675.7 nm, agreeing well with published and literature values. When compared to Chl *a* dissolved in methanol published by PhotoChemCAD (Du et al. 1998), a shift of 6 nm in peak wavelength was observed (Fig. 3a).

The peak intensity of aqueous solutions of Chl *a* at different concentrations, as measured with the LEDIF and the S_RF-5301 using an excitation wavelength of 405 nm, are shown in Fig. 3b and Fig. 3c. These ranges cover typical concentrations found in many natural waters. For regression profile comparison purposes the peak intensities of the instruments are normalized by the mean value of γ. LEDIF and S_RF-5301 regression profiles are in very good agreement and both instruments demonstrated excellent coefficients of determination over the fitted data. LEDIF peak intensity is a linear function of concentration up to 0.4 ppm, with a small deviation from linearity for higher concentrations up to 1 ppm. The small-drop off at higher concentration, a 4.7% difference at 1 ppm, may be attributed to inner filtering, as LEDIF has an optical pathlength of 9 mm (as opposed to 5 mm of a standard cuvette) to accommodate the physical dimensions of the six LED excitation systems. Measurement of newly prepared laboratory standards after 4 months elapsed time shows that the calibration correlation remained valid; no shift was observed in peak wavelength of Chl *a*.

Absorbance measurement

The product (α) of molar absorptivity and pathlength-corrected absorption at various concentrations of aqueous rhodamine B at its wavelength of maximum absorbance measured with LEDIF and OO are shown in Fig. 4a. The profiles of the absorbance curves

recorded by LEDIF and OO are found to be very similar. The absorption peak is observed at 552 and 550 nm with LEDIF and OO respectively; these values fall within the range of 550-554 nm (shaded region) reported by the manufacturer (Panreac).

Comparison of Beer-Lambert curves for aqueous rhodamine B from the LEDIF, S_UV-2550, and OO are shown in Fig. 4b. The LEDIF flowcell has an absorbance pathlength of 4 cm, differing from the 1 cm standard cuvette used by the S_UV-2550 and OO instruments. After pathlength correction, the absorbance measurements of S_UV-2550 and OO match very well with those of the LEDIF. Based on linear regression fitting to the Beer-Lambert curve and the absorbance pathlength of the instruments, the molar absorptivities (ε) were calculated as 0.193 cm^{-1}, 0.204 cm^{-1}, and 0.188 cm^{-1}, respectively. Individual measurements of molar absorptivity at different concentrations for the three instruments are reported in Fig. 4. Comparison of Beer-Lambert curves of the LEDIF with the OO for aqueous fluorescein are shown in Fig. 4c. After pathlength correction, the absorbance measurement of OO matches well with that of LEDIF. The molar absorptivities were calculated as 0.159 cm^{-1} and 0.165 cm^{-1}, respectively. All three instruments demonstrated excellent coefficients of determination over the fitted data.

Turbidity measurement

Turbidity measurement was demonstrated using a calibration standard made of styrene divinyl benzene copolymer beads in water (AMCO CLEAR TURBIDITY STANDARD, GFS Chemicals). Fig. 5a shows the scattered light spectra using 341 nm, 385 nm, and 405 nm excitation and various levels of turbidity, as well as the resulting calibration curves for turbidity in the 0 to 10 NTU range in Fig. 5b, using a 500 ms integration time. Turbidity as low as 0.1 NTU can be measured, demonstrating a potential application in monitoring processed drinking water, for which a typical upper limit specified by water authorities is 1 NTU (Ng et al. 2012*b*). Measurement of the same calibration standards after 3 months elapsed time shows that the calibration correlation remained valid. Fig. 5c shows that LEDIF turbidity measurements for different excitation wavelengths matched well with those of O_AF measurements. Both instruments demonstrated excellent coefficients of determination over the fitted data.

Quantum yield measurement

Fig. 6 shows the integrated fluorescence intensity measured from 400 nm to 600 nm as a function of solution absorbance, excited at 525 nm, for rhodamine B and rhodamine 6G. The quantum yield of rhodamine B is computed using Eq. 1, employing the quantum yield of rhodamine 6G in aqueous solution of 0.92 reported by Magde et al. (2002) and the gradients from the linear correlations observed in Fig. 6a. The computed value is found to be 0.32, which matches well with the value of 0.31 observed by Magde et al. (1999).

Temperature and pressure effects

Fluorescence is temperature sensitive and the temperature coefficients associated with different analytes are unique.

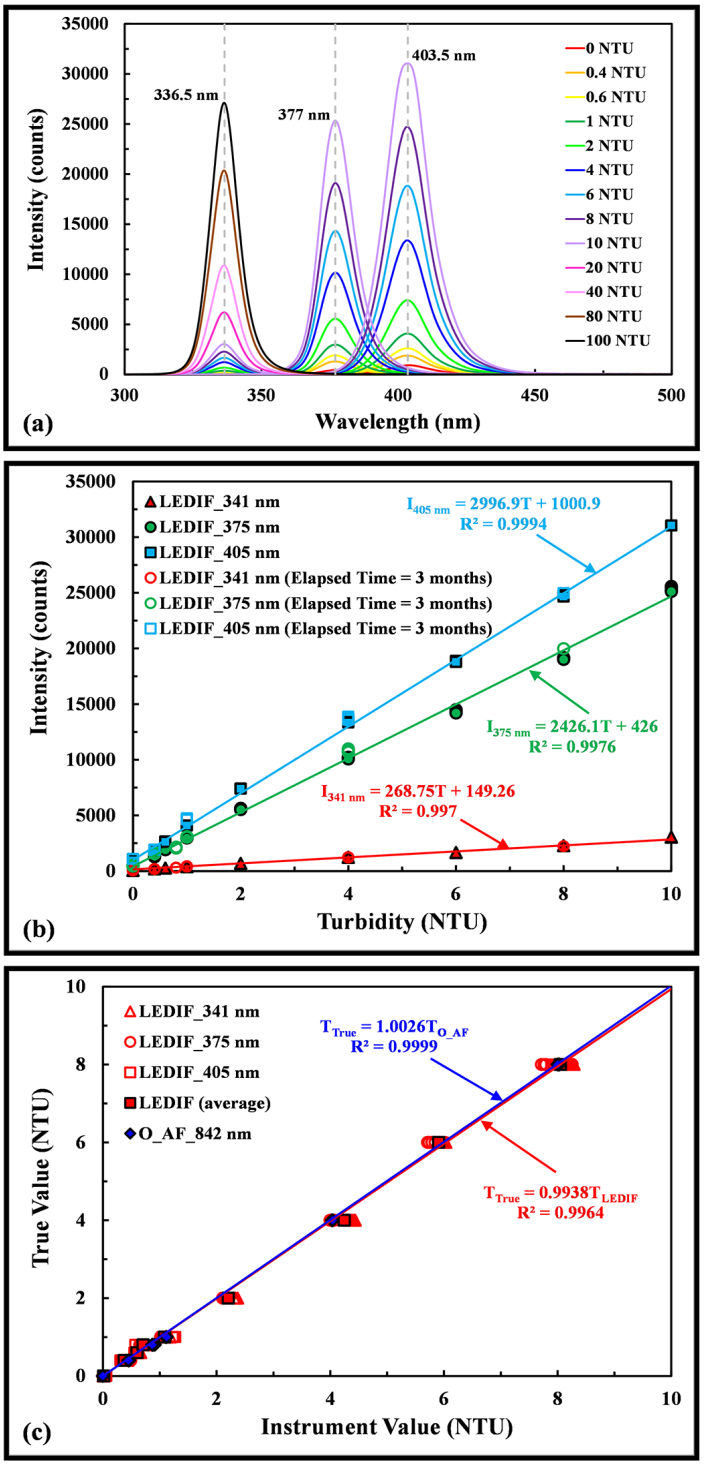

Fig. 5. Linear calibration curve for turbidity measurement of LEDIF: (a) Measurement of known turbidity standards with different excitation lights, (b) scattering of the excitation intensity of each excitation light can be calibrated and described with a single correlation for the turbidity (NTU) measurement, and (c) linear calibration of turbidity assessment measured by LEDIF and O_AF. Note: Symbol legend in instrument_light source format.

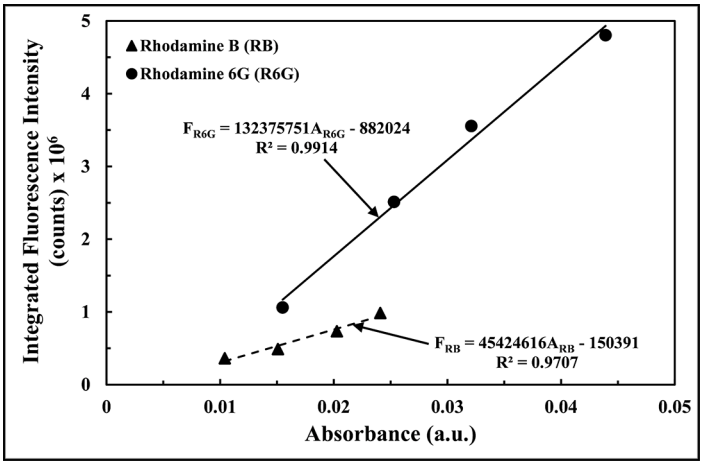

Fig. 6. Integrated fluorescence intensity as a function of absorbance measurements of LEDIF for rhodamine 6G (as reference analyte) and rhodamine B (as sample analyte) dissolved in water with an excitation wavelength of 525 nm.

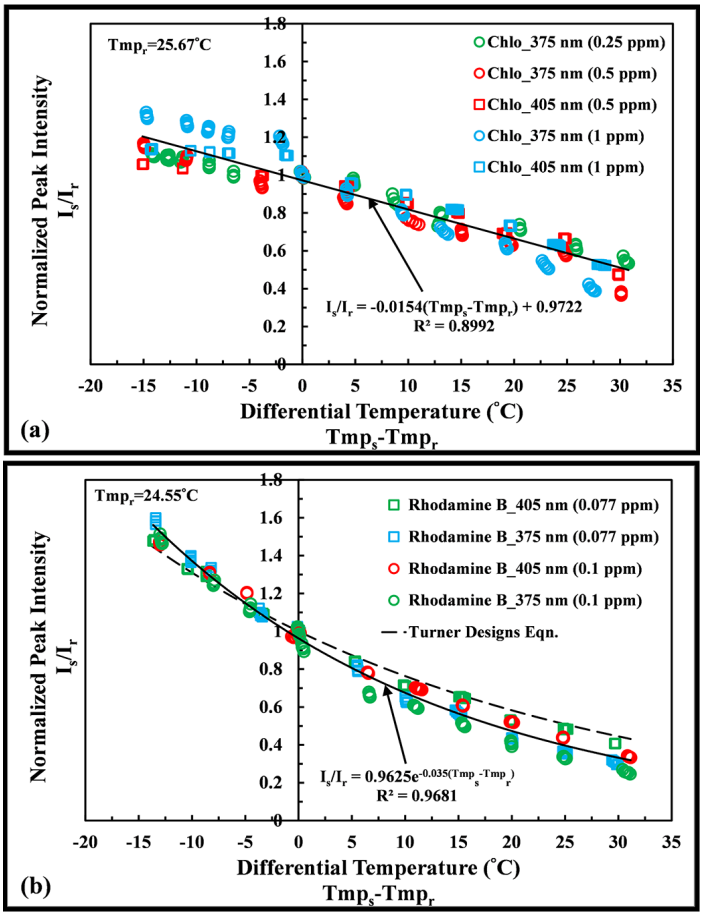

Fig. 7. Effect of temperature on fluorescence response of the LEDIF: (a) Chl *a* dissolved in water at different concentrations excited by different wavelengths of light and (b) rhodamine B dissolved in water at different concentrations excited by different wavelengths of light. Note: Symbol legend in analyte_excitation wavelength (concentration) format.

Given that LEDIF is intended for in situ measurement, the sensor response as a function of temperature was assessed using Chl *a* and rhodamine B as examples, with temperature ranging from 10°C to 55°C and with different excitation wavelengths and concentrations. Fig. 7a shows that the normalized peak intensity (I_s/I_r) of Chl *a* is a linear function of differential temperature (Tmp_s/Tmp_r) and can be described by

$$\frac{I_s}{I_r} = -0.015\left(Tmp_s - Tmp_r\right) + 0.97 \quad (7)$$

where subscripts s and r represent sample and reference readings, respectively. The linear function has a temperature coefficient of 1.5% per °C over the tested range and agrees well with the reported value of 1.4 % per °C by Turner Designs (1990). Fig. 7b shows that the normalized peak intensity (I_s/I_r) of rhodamine B can be fitted well to an exponential function of differential temperature (Tmp_s/Tmp_r) and can be described by

$$\frac{I_s}{I_r} = 0.96e^{-0.035\left(Tmp_s - Tmp_r\right)} \quad (8)$$

having an exponential temperature coefficient of 0.035 per °C over the tested range, somewhat higher than the reported temperature coefficient of 0.027 per °C reported by Turner Designs (1990).

The sensor response as a function of pressure was assessed using Chl *a* from 0 to 120 psi gauge pressure; the effect of pressure on sensor response was less than 2% over this range.

Turbidity and total suspended solids effects

Stock solutions of known concentration, AMCO CLEAR TURBIDITY STANDARD (GFS Chemicals), and cellulose powder in filtered ACS reagent grade water, certified traceable to the NIST national standard of mass (Ricca Chemical Comp) were used to prepare standards and mixtures for particle interference assessment. The turbidity standard is made up of particles having a mean diameter of 0.121 μm, ensuring permanent suspension and thus consistent light-scattering characteristics. TSS standard is made up of nonfilterable residue (cellulose powder) that has a manufacturer certified value of 95% confidence level (±2 standard deviations) and is certified traceable to NIST national mass standards. Fig. 8 assesses the effect of turbidity and TSS on observed Chl *a* fluorescence, excited at 375 nm and 405 nm. The effect of turbidity on sensor response was found to be 0.06% and 4.6%, at 375 nm and 405 nm respectively, showing the effect to be minimal up to 40 NTU. The effect of TSS on sensor response was found to be 1.6% and 6%, at 375 nm and 405 nm respectively, showing the effect to also be modest up to 50 ppm of TSS. Neither turbidity nor TSS has any effect on the fluorescence emission wavelength.

Quenching effect

Figs. 9a and 9b show the effect of static and dynamic quenching of humic acid on different concentrations of Chl *a*, excited at 375 nm and 405 nm, respectively. The association

constant of complex (k_a) and the Stern-Volmer coefficient (K_{SV}) can be determined with a 2nd order polynomial curve fit over the data and using Eq. 6. With 375 nm excitation, k_a and K_{SV} were computed as 0.00315 ± 0.0499i. With 405 nm excitation, k_a and K_{SV} were computed as 0.0004 ± 0.0490i.

Limit of detection

The instrumental detection limit (IDL) of the LEDIF is defined as: IDL = C_{sample}/{average (I)/[3σ(I)]} where C_{sample} represents concentration of sample, I denotes intensity, and σ?denotes the standard deviation of multiple measurements at this concentration. LEDIF was tested for different analytes using the available excitation wavelength closest to the absorption peak of each analyte as tabulated in Table 1. The detection limit can be improved by exciting at absorption peaks of the analyte, which is done by switching the excitation LED in use; for example, replacing the 405 nm LED with the 465 nm LED for Chl *a* measurement. Further, should a single fluorescent analyte be dominant in a specific test, the fluorescent signal could be increased by simultaneously running as many as all six LED optical systems.

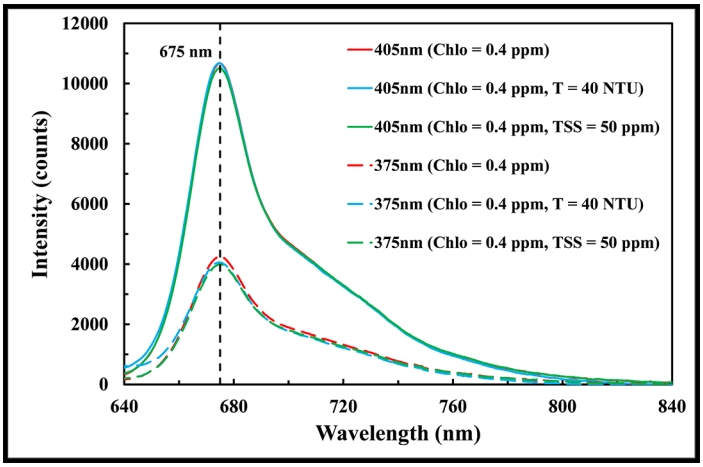

Fig. 8. Effect of particle interference due to turbidity and TSS on fluorescence response of Chl *a* dissolved in water measured with LEDIF at different excitation wavelengths. Note: Symbol legend in excitation wavelength (Chl *a* concentration, turbidity, or TSS concentration) format.

Long-term field deployment

Fig. 10 shows the temporal trend of Chl *a* (without temperature compensation) during various periods for the demonstration of LEDIF field capability. The hourly data shows that Chl *a* varied diurnally and correlated with the ambient light condition. An expanded time scale for a typical data set on a dry day,

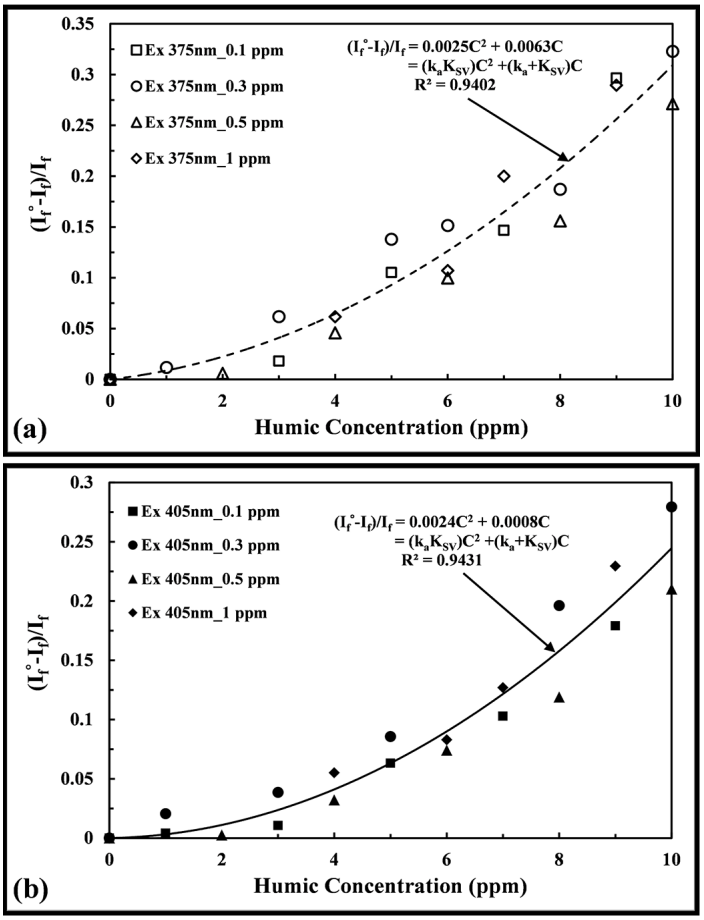

Fig. 9. Effect of static and dynamic quenching of humic on different concentrations of Chl *a*: (a) Excited at 375 nm and (b) excited at 405 nm. Note: Symbol legend in excitation wavelength_chl *a* concentration format. The association of constant of complex (k_a) and the Stern-Volmer coefficient (K_{SV}) can be computed from the coefficients of correlation.

Table 1. LEDIF instrumental detection limit (IDL) of various analytes.

Class	Analytes	Excitation wavelength (nm)	IDL* (ppb or μg/L)	IDL† (ppb or μg/L)
Pigment	Chl *a*	405	1.70	0.28
DOC	Humic		14.10	2.35
Semi Volatile	Naphthalene	285	1.20	0.20
PAH	Pyrene	260	0.20	0.03
Tracer	Rhodamine B		0.43	0.07
Tracer	Rhodamine 6G	405	0.16	0.03
Tracer	Fluorescein		0.09	0.01

*Test performed using excitation wavelength of LEDIF closest to absorption peak of analyte.
†Estimated IDL for test targeting a single analyte using six LED optical systems of the same wavelength.

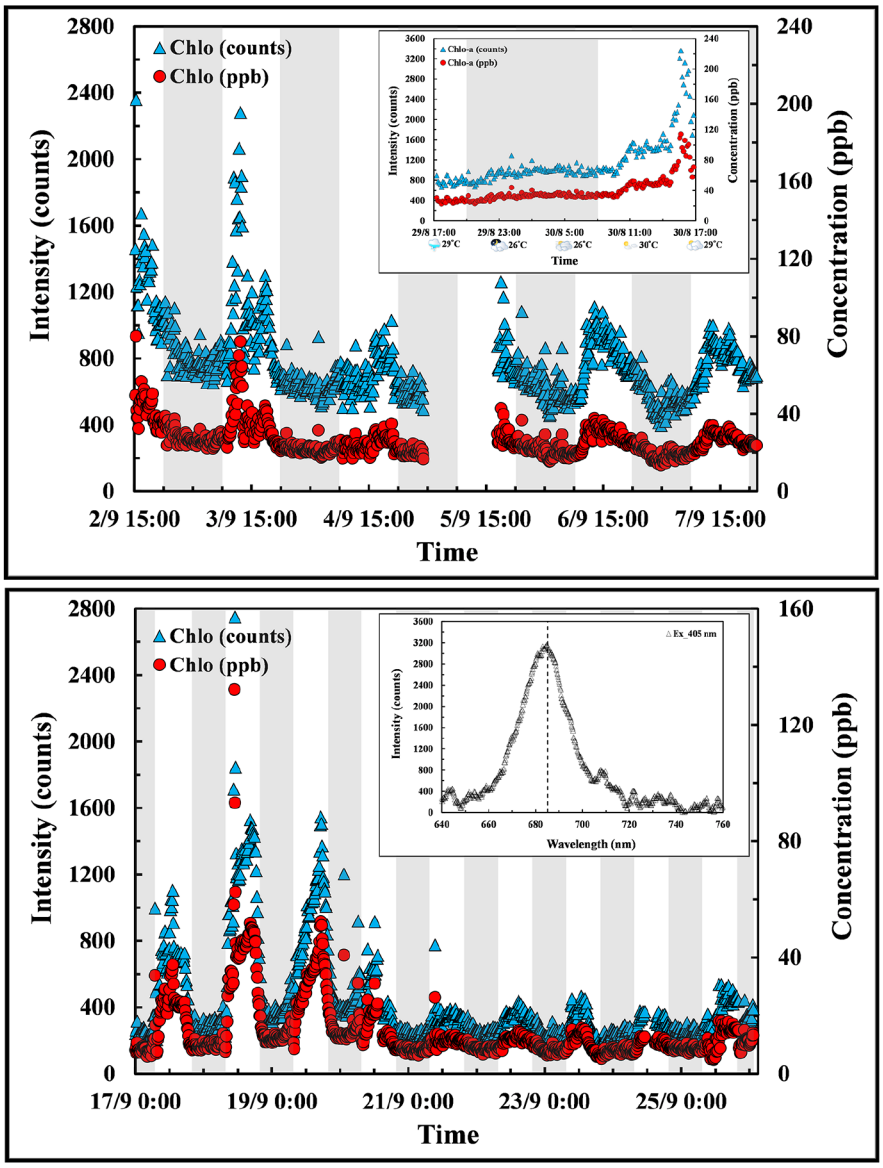

Fig. 10. Temporal trend of Chl *a* of various periods: (a) Wet and dry week data. During wet day, water flew from the pond to the lake. During dry day, the flow was significantly reduced. Insert graph shows 24 h data of an arbitrarily chosen dry day. (b) Dry week data. White and gray shaded areas represent day and night hours.

29 Aug 2013, (insert of Fig. 10a) shows that the Chl *a* concentration dropped to baseline at night. In the morning (AM), Chl *a* concentration began to rise, reached its peak in mid-afternoon (PM), and then fell back to baseline concentration in late afternoon. Maximum light intensity at the sampling location occurred in mid-afternoon due to partially shading by the stone bridge in the morning. Weekly data suggests that the Chl *a* concentration is also correlated with weather conditions. A period of seven dry days was associated with the highest values of the daytime maxima of Chl *a*, as shown in Fig. 11b. A prolonged period of wet weather corresponded to a lowering of Chl *a* concentration, possibly due to dilution by inflow from the connecting water bodies or lower levels of light.

The diurnal fluctuations are too rapid to plausibly be the result of growth and death rates of phytoplankton, and thus appear likely to be the result of horizontal or vertical movement of cells. Motile organisms may migrate diurnally to optimize illumination or minimize predation. It is noted that the daytime maxima of Chl *a* tend to be observed despite the absence of temperature compensation, which if employed would tend to show even higher daytime peaks.

Fig. 12 shows the temporal trend of turbidity of various periods. The pattern does not appear to be correlated with Chl *a*, suggesting that algae are not primarily responsible for turbidity in these waters. A typical data set on a dry day, 29 Aug 2013 (insert of Fig. 12b), shows that the variation of turbidity

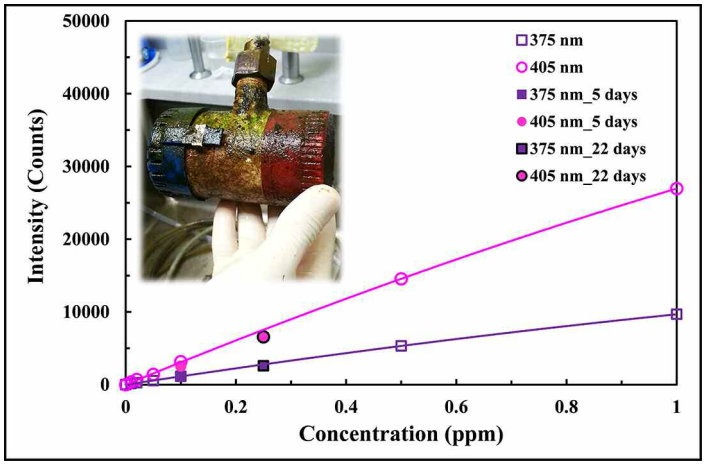

Fig. 11. Baseline measurements of Chl *a* laboratory samples of different concentration measured on the fifth and 22nd days after field deployment; showing that the effect of fouling on LEDIF measurement was modest. Insert photo shows significant fouling on bilge pump after several weeks of deployment. Note: Symbol legend in excitation wavelength_elapsed time format.

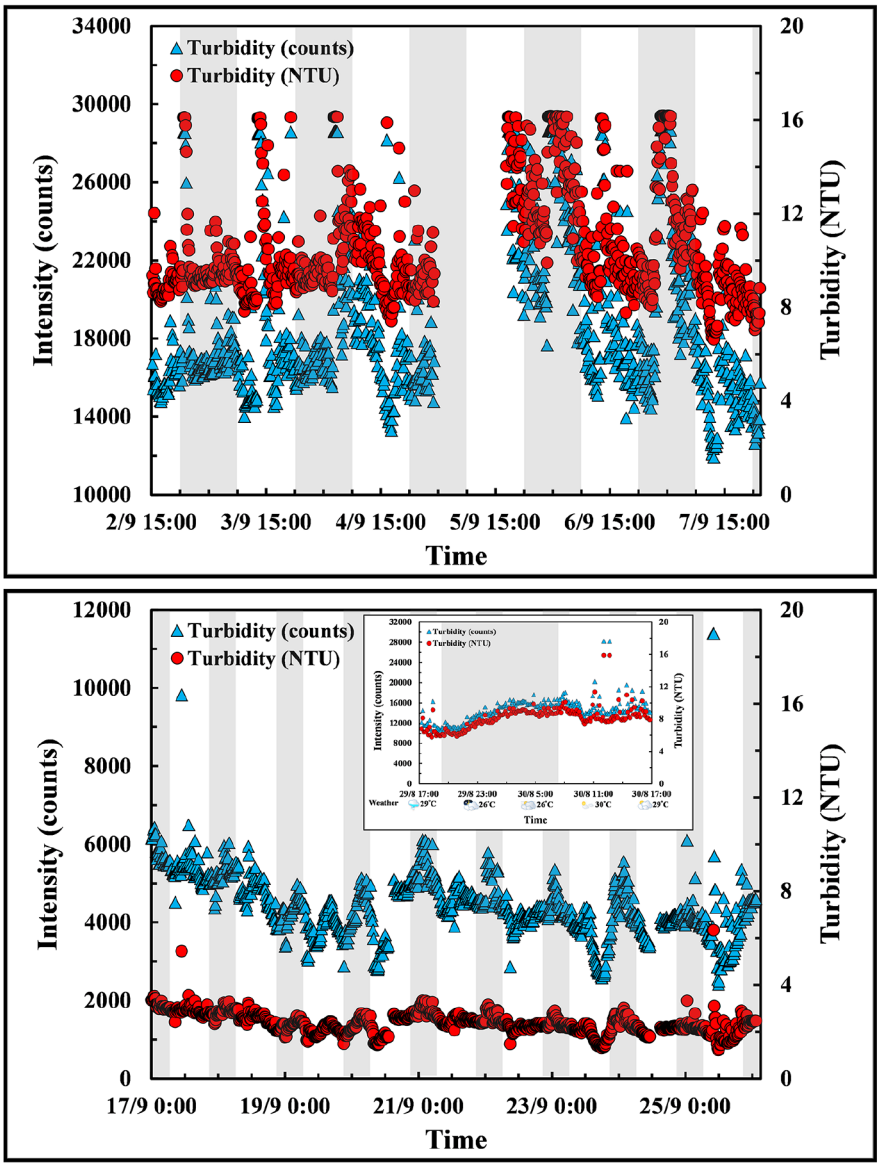

Fig. 12. Temporal trend of turbidity of various periods: (a) Wet and dry week data. (b) Dry week data. At the test site, turbidity is mostly dependent on weather contributed flow conditions.

is modest. The isolated random spiking may be attributed to aquatic life (fish, tortoise, and monitor lizard) disturbing the sediments at the water inlet, a phenomenon that has been visually observed. Weekly data suggest the turbidity is also dependent on weather conditions (e.g., dry or wet weather). For dry days, water velocity at the bridge site tended to be relatively low, tending to minimize resuspension of the sediments and perhaps thereby lowering turbidity values. For wet day, water flows from the pond to the main lake may stir up sediments and result in higher turbidity measurements.

Discussion

The LEDIF is demonstrated to correctly measure fluorescence, optical absorbance, and light scattering, and can also be used to determine quantum yield. The LEDIF can be built at moderate cost using mostly off-the-shelf components; the materials bill for the unit tested here was approximately $12,500 Singapore (order of $10,000 US). Power consumption (0.5 W and 1 W in idle mode, without and with wifi/3G/4G communications, respectively; <11 W in all active measurement modes) is low enough that a compact (4[L] × 10[W] × 8[H] cm) Li-ion rechargeable battery of 110 Wh would have sufficient to power LEDIF for a day during the current field tests.

Comments and recommendations

A solar panel could be used to power LEDIF for off-grid long-term sensing. Assuming that the LEDIF runs every hour for a duration of 3 min, and assuming a requirement of 3 days of autonomy, a pair of 110 Wh Li-ion batteries having dimensions of (8[L] × 10[W] × 4[H] cm) would suffice. A 120 W solar panels would be appropriate for a tropical day-light regime. The flowcell was demonstrated to withstand >10 bars of pressure without leakage; higher pressure versions are doubtless possible by using thicker quartz windows if it were desired to monitor high-pressure waters. For longer unserviced deployments a software controlled compressed air cleaning system could be implemented to suppress fouling in the fluid transportation manifold. Finally, inclusion of a low cost temperature sensor could be easily incorporated to the LEDIF for temperature measurements and fluorescence corrections if it is desirous to achieve greatest accuracy.

Acknowledgments

Funding for this work was provided by the Singapore National Research Foundation (NRF) through the Singapore-MIT Alliance for Research and Technology (SMART) Center for Environmental Sensing and Modeling (CENSAM). We thank Jurong Town Council (JTC) Corporation and SMM Pte Ltd of Jurong International for their support in furnishing test site for this work. We thank S. Senft-Grupp for advice and helpful discussions and S. Z. Binte Kamis for feedback on sensor usage. Patent Applications for Singapore, China, and United States have been filed by Ng et al. (2013), based on the claims of international Patent Corporation Treaty Application PCT/SG2012/000142 filed by Ng et al. (2012*a*).

References

Atkinson, S. F., and J. A. Mabe. 2006. Near real-time monitoring and mapping of specific conductivity levels across Lake Texoma, USA. Environ. Monit. Assess. 120:449-460 [doi:10.1007/s10661-005-9072-x].

Chow, C., R. Fabris, and M. Dixon. 2008. Case studies using S::SCAN on-line monitoring system. Research Report 75. Water Quality Research Australia, Adelaide.

de Hoogh, A., J. Wagenvoort, F. Jonker, J. A. Van Leerdam, and A. C. Hogenboom. 2006. HPLC-DAD and Q-TOF MS techniques identify cause of Daphnia biomonitor alarms in the river. Meuse. Environ. Sci. Technol. 40:2678-2685 [doi:10.1021/es052035a].

Du, H., R. A. Fuh, J. Li, A. Corkan, and J. S. Lindsey. 1998. PhotochemCAD: A computer-aided design and research tool in photochemistry. Photochem. Photobiol. 68:141-142.

Hohman, B. 2007. Challenge studies of the pittsburgh distribution network pilot contamination warning system. Univ. of Pittsburgh.

Jeon, J., J. H. Kim, B. C. Lee, and S. D. Kim. 2008. Development of a new biomonitoring method to detect the abnormal activity of Daphnia Magna using automated grid counter device. Sci. Total Environ. 389:545-556 [doi:10.1016/j.scitotenv.2007.09.015].

Lakowicz, J. R. 2006. Principles of fluorescence spectroscopy, 3rd ed. Springer [doi:10.1007/978-0-387-46312-4].

Magde, D., G. E. Rojas, and P. G. Seybold. 1999. Solvent dependence of the fluorescence lifetimes of xanthene dyes. Photochem. Photobiol. 70:737-744 [doi:10.1111/j.1751-1097.1999.tb08277.x].

———, R. Wong, and P. G. Seybold. 2002. Fluorescence quantum yields and their relation to lifetimes of phodamine B and fluorescein in nine solvents: improved absolute standards for quantum yields. Photochem. Photobiol. 75:327-334 [doi:10.1562/0031-8655(2002)075<0327:FQYATR>2.0.CO;2].

Manov, D. V., G. C. Chang, and T. D. Dickey. 2003. Methods for reducing biofouling of moored optical sensors. J. Atmos. Ocean. Technol. 21:958-968 [doi:10.1175/1520-0426(2004)021<0958:MFRBOM>2.0.CO;2].

Mons, M. 2008. Monitoring and control of drinking water quality—Inventory and evaluation of monitoring technologies for key-parameters. Techneau Report.

Ng, C. L., H. F. Hemond, and S. Senft-Grupp. 2012*a*. Highly compact multi-optical-junction optical flowcell and flexibly deployable optical sensing assemblies and systems for in-situ real-time spectroscopic measurements. International Patent Corporation Treaty Application. PCT/SG2012/000142.

———, S. Senft-Grupp, and H. F. Hemond. 2012*b*. A multi-platform optical sensor for in situ sensing of water chem-

istry. Limnol. Oceanogr. Methods 10:978-990 [doi:10.4319/lom.2012.10.978].

———, H. F. Hemond, and S. Senft-Grupp. Date of filing: 21 Oct 2013. Highly compact multi-optical-junction optical flowcell and flexibly deployable optical sensing assemblies and systems for in-situ real-time spectroscopic measurements. Singapore Patent Application 201307797-9, China Patent Application, and US Patent Application 14/113026.

Sengupta S., M. Mujacic, and E. J. Davis. 2006. Detection of bacteria by surface-enhanced raman spectroscopy. Anal. Bioanal. Chem. 386:1379-1386 [doi:10.1007/s00216-006-0711-z].

Storey, V. M., B. V. Gaag, and B. P. Burns. 2011. advances in online drinking water quality monitoring and early warning systems. Water Res. 45:741-747 [doi:10.1016/j.watres.2010.08.049].

Turner Designs. 1990. Fluorometric facts: A practical guide to flow measurement, p. 18. <http://www.turnerdesigns.com/t2/doc/appnotes/998-5000.pdf>

U.S. EPA. 2009. Distribution system water quality monitoring: sensor technology evaluation methodology and results. EPA/600/R-09/076, Washington, D.C.

U.S. EPA. 2010. Detection of biological suspensions using online detectors in a drinking water distribution system simulator. EPA/600/R-10/005, Washington, D.C.

Van den Broeke, J. 2005. A short evaluation of the S::can Spectro::lyser. KIWA Water Research.

Van der Gaag, B., and J. Volz. 2008. Real-time on-line monitoring of contaminants in water: Developing a research strategy from utility experiences and needs. KIWA Water Research.

Weber, G. 1948. The quenching of fluorescence in liquids by complex formation. determination of the mean life of the complex. Trans. Faraday Soc. 44:185-189 [doi:10.1039/tf9484400185].

Williams, A. T. R., S. A. Winfield, and J. N. Miller. 1983. Relative fluorescence quantum yields using a computer controlled luminescence spectrometer. Analyst 108:1067-1071 [doi:10.1039/an9830801067].

Xie, C., J. Mace, M. A. Dinno, W. Q. Li, W. Tang, R. J. Newton, and P. J. Gemperline. 2005. Identification of single bacterial cells in aqueous solution using confocal laser tweezers raman spectroscopy. Anal. Chem. 77:4390-4397 [doi:10.1021/ac0504971].

Zurita, J. L., A. Jos, A. M. Cameán, M. Salguero, M. López-Artíguez, and G. Repetto. 2007. Ecotoxicological evaluation of sodium fluoroacetate on aquatic organisms and investigation on the effects of wofish cellines. Chemosphere 67:1-12 [doi:10.1016/j.chemosphere.2006.10.027].

Submitted 20 January 2014
Revised 24 April 2014
Accepted 22 June 2014